PAPER

Excited-state properties of chiral [4]helicene cations†

Oksana Kel,[a] Peter Sherin,[a,b] Nathalie Mehanna,[c] Benoît Laleu,[c] Jérome Lacour*[c] and Eric Vauthey*[a]

The photophysical properties of a series of helicene cations in various solvents have been investigated using stationary and time-resolved spectroscopy. These compounds fluoresce in the near infrared region with a quantum yield ranging between 2 and 20% and a lifetime between 1 and 12 ns, depending of the solvent. No clear solvent dependence could be recognized except for a decrease of fluorescence quantum yield and lifetime with increasing hydrogen-bond donating ability of the solvent. In water, the helicene cations undergo aggregation. This effect manifests itself by the presence of a slow fluorescence decay component, whose amplitude increases with dye concentration, and by a much slower decay of the polarization anisotropy in water compared to an organic solvent of similar viscosity. However, aggregation has essentially no effect on the stationary fluorescence spectrum, whereas relatively small changes can be seen in the absorption spectrum. Analysis of the dependence of aggregation on the dye concentration reveals that the aggregates are mostly dimers and that the aggregation constant is substantially larger for hetero- than homochiral dimers.

Introduction

There is a growing need for near-infrared (NIR) fluorescent probes for numerous applications in chemistry, biochemistry and medicine.[1–5] It is indeed well-known that the efficiency of single molecule detection is significantly better with NIR than with visible fluorophores, even though the former are normally characterized by a smaller fluorescence quantum yield and lifetime.[6] This superior detection efficiency mainly arises from the lower emission background upon excitation with NIR light, which is not absorbed by fluorescent impurities. Another advantage of a long excitation wavelength is that IR light is less energetic than visible light and thus causes less damage to biological tissues, a crucial factor for living cell imaging applications.

Here we report on our investigation of the photophysical properties of a series of new [4]helicene cation (HelR) derivatives (Chart 1) that emit in the NIR region.[7–14] These compounds belong to the class of intrinsically chiral aromatic molecules called "helicenes", which have been intensively studied over the last decade owing to their promising photochromic,[15,16] and non-linear optical properties.[17–20] HelR derivatives are, against conventional wisdom, highly configurationally stable helicenes due to strong steric repulsions between the methoxy substituents in

positions 1 and 13, and the large degree of rigidity brought by the two nitrogen atoms in conjugation.[9,21] In fact, a rather high barrier of racemization has been measured previously for HelPr derivatives ($\Delta G^{\ddagger}$ = 41.3 kcal mol^{-1} at 200 °C). Beside this, their molecular shape and extended aromaticity give them the ability to bind to biological macromolecules. It has been shown that the (*P*)-enantiomer of a helicene bearing a protonated amino group exhibits structural selectivity for binding to DNA and discriminates between right-handed B-DNA and left-handed Z-DNA.[22] DNA-binding properties have also been demonstrated with 5,8-bis(aminomethyl)-1,12-dimethylbenzo[c]-phenanthrene and N-methyl-5-azahelicenium salts.[23,24] Since it is commonly established that a positive charge on an aromatic molecule enhances its binding ability to DNA,[25] the HelR dyes can be expected to bind to DNA and to have thus some potential as NIR fluorescent DNA probes.

In addition to the aforementioned properties, self-assembling is a common feature of helicenes. Heterocyclic helicenes have been shown to assemble into hexagonal phases consisting of hollow-centred helical columns.[26,27] A similar helical columnar liquid–crystalline structure is typical for other materials such as DNA,[28] poly(γ-benzyl-L-glutamate),[29] and xanthan.[30] Enantiopure helicenamidate was grafted on to silica nano-particles and

[a]*Department of Physical Chemistry, University of Geneva, CH-1211 Geneva 4, Switzerland. E-mail: eric.vauthey@unige.ch*
[b]*International Tomography Center SB RAS, Institutskaya str. 3a, 630090 Novosibirsk, Russia*
[c]*Department of Organic Chemistry, University of Geneva, CH-1211 Geneva 4, Switzerland. E-mail: jerome.lacour@unige.ch*

†Electronic supplementary information (ESI) available: Synthesis of HelOH, absorption and emission spectra of HelPr in CHCl$_3$ at different concentrations, and fluorescence decays of HelPr in CHCl$_3$ at different wavelengths. See DOI: 10.1039/c2pp05361f
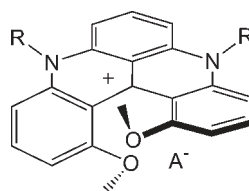
HelMe: R=CH$_3$, A$^-$=BF$_4^-$, Cl$^-$
HelPr: R=(CH$_2$)$_2$CH$_3$, A$^-$=Cl$^-$
HelOH: R=(CH$_2$)$_2$OH, A$^-$=CF$_3$COO$^-$

Chart 1 (*M*)-HelR dyes.

the resulting nanostructure showed the ability to aggregate and de-aggregate in different aromatic solvents.[31] The chirality of stereoisomers of a cyclic alkyne containing three helicene units was found to play an important role in their self-aggregations.[32]

Although the number of studies on this class of molecule is increasing, photophysical investigations, apart from basic absorption and emission spectroscopy,[24,27,33,34] are still very scarce.[35–37]
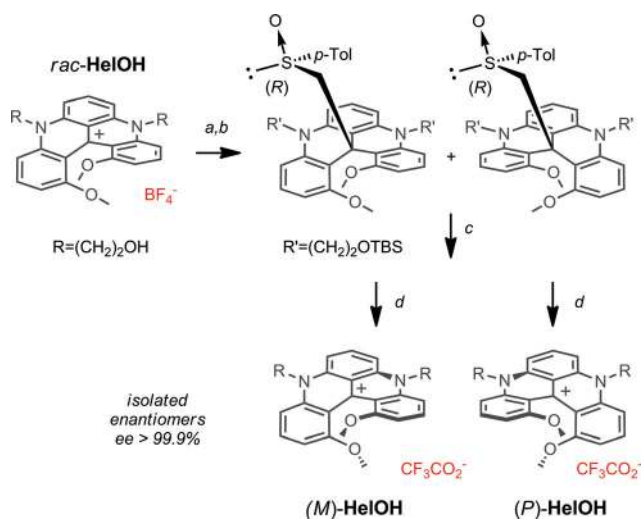
We present here a detailed photophysical investigation of the HelR dyes using stationary, as well as time-resolved, absorption and emission spectroscopy with femtosecond resolution. Special attention has been devoted to the aggregation of these compounds as well as to the photophysical properties of the aggregates.

Experimental

Samples

All racemic HelR dyes were synthesized according to literature procedures.[7,8,38] Enantiopure HelMe and HelPr have been described previously.[9,10,14] For the preparation of (M)- and (P)-HelOH, the following four-step procedure was utilized (Scheme 1 and ESI†). First, the two terminal hydroxyl groups of rac-HelOH were capped with t-butyldimethylsilyl groups. The resulting carbenium ion was reacted with the carbanion of (R)-p-tolyl-methylsulfoxide.[39,40,38,39] A facile chromatographic separation of the resulting diastereomers was followed by Pummerer fragmentation and coupled desilylation reactions affording the cations in enantiopure forms.

The organic solvents, methanol (MeOH), ethanol (EtOH), pentanol (PeOH), acetonitrile (ACN), dimethyl sulfoxide (DMSO), tetrahydrofuran (THF), dichloromethane (DCM) and chloroform ($CHCl_3$) were of the highest commercially available grade and were used as received. Phosphate buffered saline (PBS) was purchased from Invitrogen and water was doubly distilled. The aqueous solutions were prepared by dissolving 1–2 μl of a stock solution of the dye (2mM) in DMSO (stored in the dark) in 1–2 ml of non-buffered or buffered aqueous solution.

Steady-state measurements

Absorption spectra were recorded with a Cary 50 spectrophotometer, whereas fluorescence and excitation spectra were measured with a Cary Eclipse fluorimeter. All fluorescence spectra were corrected for the wavelength-dependent sensitivity of the detection. The fluorescence quantum yields of the HelR dyes were determined relative to a solution of oxazine 1 perchlorate (from Exciton) in ethanol, $\Phi_f = 0.11$.[41]

Time-resolved fluorescence

Fluorescence lifetime measurements on the nanosecond time-scale were performed with a time-correlated single photon counting (TCSPC) setup described in detail elsewhere.[42] Excitation was carried out at 395 nm with a laser diode (Picoquant model LDH-P-C-400B) generating ~60 ps pulses at 10 MHz. The instrument response function (IRF) had a full-width at half-maximum (FWHM) of about 200 ps.
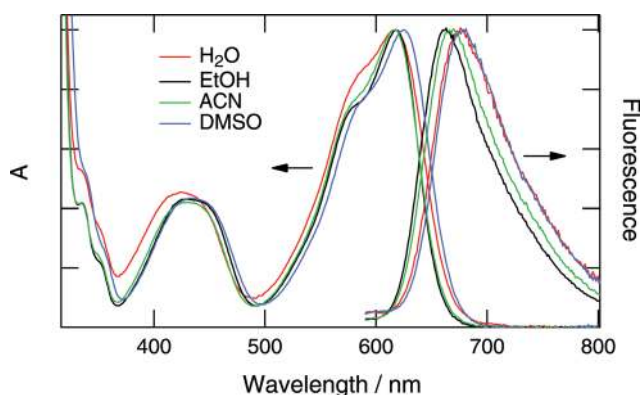
The fluorescence dynamics of the HelR dyes on a shorter timescale was measured by fluorescence up-conversion (FU). As discussed previously,[43,44] excitation was achieved at 400 nm with the frequency-doubled output of a Kerr lens mode-locked Ti:sapphire laser (Mai Tai, Spectra-Physics). The polarization of the pump pulses was at magic angle relative to that of the gate pulses at 800 nm. The pump intensity on the sample was of the order of 5 μJ cm^{-2} and the FWHM of the IRF was ca. 210 fs. The sample solutions were located in a 1.0 mm rotating cell and had an absorbance of about 0.2 at 400 nm.

Transient absorption (TA)

The experimental setup was the same as that described in the literature.[45,46] Excitation was performed either at 400 nm with the frequency-doubled output of a standard 1 kHz amplified Ti:sapphire system (Spectra-Physics) or at 600 nm with a home-built two-stage non-collinear optical parametric amplifier. The pump intensity on the sample was about 1–2 mJ cm^{-2}. The polarization of the probe pulses was at magic angle relative to that of the pump pulses. All spectra were corrected for the chirp of the white-light probe pulses. The FWHM of the IRF was ca. 200 fs. The sample solutions were placed in a 1 mm thick quartz cell and were continuously stirred by N_2 bubbling. Their absorbance at the excitation wavelength was around 0.3.

Quantum chemical calculations

Ground-state gas-phase geometry optimization was performed at the density functional level of theory (DFT) using the B3LYP functional,[47] and a [3s2p1d] basis set.[48] Electronic vertical excitation energies were computed with time-dependent density functional theory (TD-DFT) using the same functional and basis

Scheme 1 Four-step resolution protocol of HelOH: (a) t-butylchlorodimethylsilane, imidazole, DMF, 25 °C, 24 h, 65%; (b) (+)-(R)-methyl-p-tolylsulfoxide, LDA, THF, 0 °C; (c) diastereomer separation by chromatography (SiO_2, Et_2O) 45 and 49% (two-steps); (d) TFAA, CH_2Cl_2, 25 °C, 85%.

Fig. 1 Absorption and fluorescence spectra of (*rac*)-HelMe in various solvents.

set.[49] The calculations were carried out using Turbomole version 6.0.[50]

Results and discussion

HelR dyes in organic solvents

The photophysics of the HelR derivatives in aqueous solutions differs substantially from that in organic solvents and will thus be discussed separately. The UV-vis absorption spectra of the dyes in organic solvents show two bands in the visible region with maxima around 617 and 425 nm (Fig. 1), whereas the fluorescence spectra consist of a single band centred between 650 and 690 nm depending on the R-substituent and the solvent (Table 1).

TD-DFT calculations of the HelR dyes in the gas phase predict the first electronic transition to be at 530 nm and to be due to a HOMO–LUMO one-electron transition (Table 2). Fig. 2 shows that this transition involves a decrease of electron density at R and an increase at the methoxy-oxygen atom. Thus this first transition has some charge transfer character. This could explain why its energy calculated in the gas phase is substantially larger than that measured in solutions. Unfortunately, because of their ionic nature, the absorption spectrum of the HelR dyes cannot be measured in weakly or non-polar solvents. According to the calculations, the absorption band observed around 425 nm should be due to two transitions of similar intensity but with a rotatory

Table 1 Absorption, λ_a, and fluorescence, λ_f, maxima of the (rac)-HelR dyes in various solvents

| Solvent	λ_a (nm)			λ_f (nm)		
	HelMe	HelPr	HelOH	HelMe	HelPr	HelOH
H_2O	614	617	615	678	677	680
MeOH	615	617	617	664	663	673
EtOH	617	618	618	663	662	672
PeOH	619	619	621	664	663	672
ACN	615	617	617	671	668	678
DMSO	625	625	627	683	677	690
THF	619	620	621	668	665	678
DCM	616	617	619	658	656	672
$CHCl_3$	616	617	621	662	658	679

Table 2 Spectroscopic parameters obtained from the TD-DFT calculations of the HelR dyes in the gas-phase

	HelMe	HelPr	HelOH
$S_1 \leftarrow S_0$ transition			
E^a (eV)	2.35	2.35	2.34
	HOMO–LUMO	HOMO–LUMO	HOMO–LUMO
μ^b (D)	$\mu_y = -3.16$	$\mu_y = -3.55$	$\mu_y = -3.45$
	$\mu_z = -0.50$	$\mu_z = -0.60$	$\mu_z = -0.55$
R^c (a.u.)	3.9×10^{-4}	1.2×10^{-4}	1.8×10^{-4}
$S_2 \leftarrow S_0$ transition			
E (eV)	2.72	2.77	2.73
	HOMO-1–LUMO	HOMO-1–LUMO	HOMO-1–LUMO
μ (D)	$\mu_x = -2.30$	$\mu_x = -2.28$	$\mu_x = -2.30$
R (a.u.)	-1.2×10^{-3}	-1.1×10^{-3}	-1.1×10^{-3}
$S_3 \leftarrow S_0$ transition			
E (eV)	2.88	2.88	2.84
	HOMO-2–LUMO	HOMO-2–LUMO	HOMO-2–LUMO
μ (D)	$\mu_y = 2.64$	$\mu_y = 2.50$	$\mu_y = 2.69$
	$\mu_z = -0.90$	$\mu_z = -0.88$	$\mu_z = -0.90$
R (a.u.)	5.4×10^{-4}	5.5×10^{-4}	5.0×10^{-4}

[a] Energy. [b] Transition dipole moment. [c] Rotatory strength (*P*-form) in atomic units.
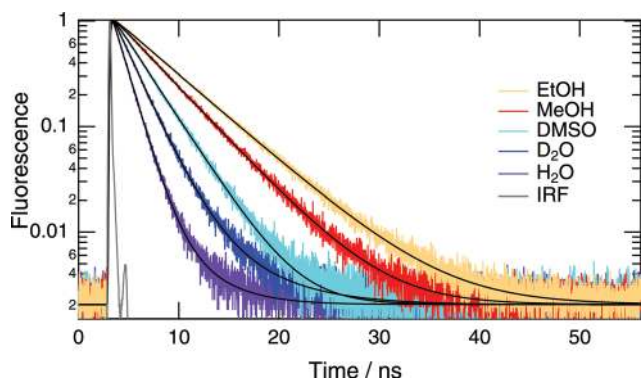
strength of opposite sign. This prediction agrees very well with the circular dichroism spectra of HelMe, that shows one band at 407 nm with the same sign as that of the 625 nm band, and one band at 456 nm with opposite sign.[51]

The fluorescence dynamics of the dyes in organic solvents was recorded at 670 nm upon 395 nm excitation. In most cases, the fluorescence time profiles, some of which being shown in Fig. 3, could be reproduced well using an exponential function convolved with the IRF and with the time constants, τ_f, listed in Table 3. However, the sum of two exponential functions was
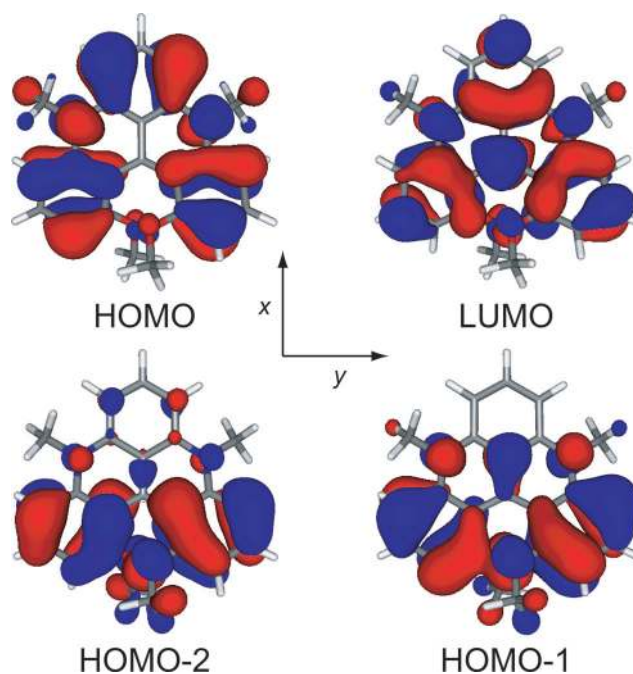
Fig. 2 Frontier molecular orbitals of HelMe computed at the B3LYP/[3s2p1d] level of theory. Orbital contours are drawn at the 0.02 a.u. level.

This journal is © The Royal Society of Chemistry and Owner Societies 2012

Photochem. Photobiol. Sci., 2012, **11**, 623–631 | 625

Fig. 3 Intensity normalized fluorescence time profiles measured with (*rac*)-HelPr in different solvents, instrument response function (IRF) and best fits (black lines).

required for all three compounds in CHCl$_3$ and for HelOH in DCM. Measurements at different wavelengths (670, 690 and 780 nm) revealed an increasing contribution of the short-lived component at longer wavelengths (Figure S1, ESI†). Such decay points to the existence of two emitting species with slightly different spectra.

Whereas the shape of the absorption spectrum of the dyes in CHCl$_3$ is independent of concentration, a noticeable red shift of the fluorescence band, that is not due to reabsorption, takes place with increasing concentration (Figure S2, ESI†). Moreover, the relative amplitude associated with the shortest lifetime increases markedly with increasing concentration (Table S1, ESI†). This concentration dependence suggests that an HelR excimer or an excited aggregate is most probably responsible for the red-shifted emission with the shortest lifetime. Unfortunately, the spectra associated with the two decay components overlap too much to allow the observation of precursor–successor kinetics, as expected the case of excimer, and to permit an unambiguous assignment. Excimers formation is typical of many aromatic hydrocarbons,[52,53] but the excimer band is usually much more

red-shifted compared to that of the monomer and the lifetime is also substantially longer. As it will be shown below, aggregation of the HelR dyes plays a dominant role in aqueous solution, where it is mainly driven by hydophobic effects. A limited solubility of the HelR dyes in DCM and CHCl$_3$, which are the least polar solvents used here, could also result to the formation of aggregates.

The non-radiative rate constants, k_{nr}, calculated from the fluorescence lifetimes and quantum yields, Φ_f, are listed in Table 3. Whereas the radiative rate constant, k_r, is essentially solvent independent, around 1–1.5×10^7 s^{-1}, k_{nr} varies substantially. Despite this, no evident relationship between τ_f or k_{nr} and a solvent property or a solvatochromic scale (Lippert–Mataga, E$_T$(30), Kamlet–Taft)[54] can be recognized. However, if only alcohols are considered, a substantial increase of the fluorescence lifetime of all three HelR dyes with increasing alkyl chain length can be observed. As the hydrogen-bond donating properties of the alcohols is also decreasing in the same order, this points to the possible involvement of intermolecular hydrogen bond assisted non-radiative deactivation. This point will be considered further below when discussing the photophysics of the HelR dyes in aqueous solutions. However, the shorter lifetime in DMSO and ACN compared to EtOH clearly shows that other factors play a role in the non-radiative transition of these compounds. Additionally to this variation with the solvent, Table 3 also reveals that the R-substituents have a clear influence on τ_f and that this effect originates from k_{nr}, which increases in the order R = Pr, Me, CH$_2$CH$_2$OH in all organic solvents. Whereas, the shorter lifetime with HelOH could possibly arise from hydrogen-bond interaction with the solvent, we do not have any reasonable explanation for the difference between HelMe and HelPr. However, it should be noted that the counter-ion was different for all three compounds (Chart 1).

The TA spectra of all three HelR derivatives have been measured in EtOH at different delays after 600 and 400 nm excitation. The resulting spectra are essentially independent of the excitation wavelength and of R, those measured with HelPr upon

Table 3 Photophysical properties of the HelR dyes in various solvents

Solvent	(*rac*)-HelMe			(*rac*)-HelPr			(*M*)-HelOH		
	$\Phi_f\,10^2$	τ_f (ns)	$k_{nr}^{\,a}$ (ns^{-1})	$\Phi_f\,10^2$	τ_f (ns)	$k_{nr}^{\,a}$ (ns^{-1})	$\Phi_f\,10^2$	τ_f (ns)	$k_{nr}^{\,a}$ (ns^{-1})
PBS	1.9	1.3 3.7	0.75	2.6	1.6 4.7	0.60	1.6	1.2 5.3	0.85
H$_2$O	1.9	1.3 3.6	0.75	2.5	2.0 5.0	0.50	1.6	1.1 5.2	0.86
D$_2$O	2.2	2.0 5.5	0.49	3.2	2.5 7.0	0.39	2.1	1.8 6.6	0.54
MeOH	5.2	4.3	0.22	7.4	5.6	0.17	3.5	2.8	0.34
EtOH	7.0	5.3	0.17	9.6	6.7	0.13	4.4	3.3	0.29
PeOH	8.9	6.2	0.15	11.8	7.7	0.12	5.9	4.1	0.23
ACN	5.0	4.2	0.23	7.6	5.5	0.17	3.5	2.9	0.33
DMSO	4.0	3.0	0.32	6.3	4.0	0.23	3.1	2.1	0.46
THF	7.3	5.3	0.18	10.5	7.0	0.13	4.3	3.2	0.30
DCM	17.2	11.3	0.07	20.5	12.0	0.06	5.5	3.1 6.6	0.14
CHCl$_3$	11.3	5.8 14.0	0.06	14.4	4.7 14.8	0.06	4.0	2.7 6.2	0.15

^{a} Calculated with the shortest lifetime in aqueous solution and the longest lifetime in DCM and CHCl$_3$.
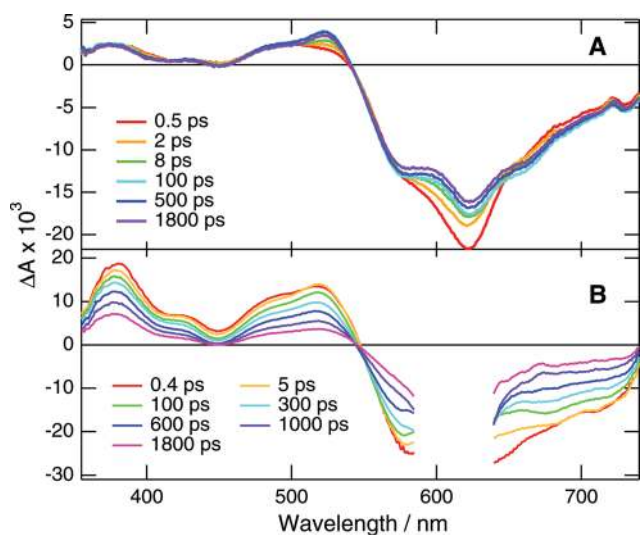
Fig. 4 TA spectra measured at various time delays after excitation of a solution of (*rac*)-HelPr in EtOH at 400 nm (A) and in aqueous buffer solution at 600 nm (B).

Fig. 5 Normalized absorption spectra of (*rac*)-HelMe at different concentrations in aqueous buffer solution.

400 nm excitation being shown in Fig. 4A. These spectra are dominated by positive bands between 600 and 540 nm and by a broad negative band below 540 nm. The positive TA bands can be assigned to absorption of the S_1 excited state overlapping with the bleach of the 425 nm ground-state absorption band. On the other hand, the broad negative band originates from both the bleach of the $S_1 \leftarrow S_0$ transition and the stimulated $S_1 \rightarrow S_0$ emission, slight differences between the steady-state absorption spectrum and the bleach signal being due to overlapping excited-state absorption. During the first 10 ps, some spectral dynamics takes place, leading to a narrowing of the 500 nm TA band together with the transformation of the shoulder at 520 nm into a maximum, as well as to a blue-shift of the 380 nm band. The time constants associated with this process, 0.5 and 12 ps, suggests that the dynamics are probably connected with vibrational and/or solvent relaxation. Once this process is over, the whole TA signal decays on the nanosecond timescale in agreement with the fluorescence lifetime discussed before. The time evolution of the TA intensity over the whole measured spectral range could be well reproduced using a sum of three exponential functions decaying to zero with 0.5 ps, 12 ps and 6.7 ns, the latter constant, taken from the TCSPC measurements, being hold fixed. This extrapolated decay to zero of the whole TA intensity indicates that intersystem-crossing (ISC) to the triplet state is not a significant deactivation pathway of the S_1 population. If it were the case, the decay of the S_1 state population would result to only a partial recovery of the ground-state population. Consequently, fluorescence and internal conversion seems to be the main S_1 state deactivation pathways of the HelR dyes in organic solvents.

HelR dyes in aqueous solutions

The absorption spectra of the HelR dyes in water, D_2O and aqueous buffer solutions differ from those in organic solvents by the larger width of the $S_1 \leftarrow S_0$ band, the more marked shoulder around 580 nm, as well as by the blue shift of the 425 nm band
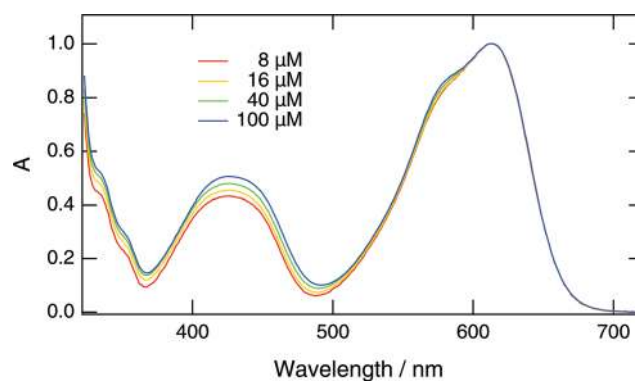
(700 cm^{-1} relative to ACN) (Fig. 1). As depicted in Fig. 5, the relative intensity of the first two absorption bands varies with the dye concentration. Moreover, the 580 nm shoulder becomes more pronounced as the HelR concentration increases. These effects point to the formation of HelR aggregates in aqueous solutions.

The emission spectra of all three HelR dyes in aqueous solution are similar to those in organic solvents (Fig. 1) with the band maximum located between 677 and 680 nm depending on R. As expected, the enantiomers and racemic mixtures of each compound have the same fluorescence quantum yield (Table 3), but the latter are substantially smaller than in organic solvents. The increase of Φ_f by a factor of about 1.3 on going from water to deuterated water points to the involvement of intermolecular hydrogen bonds in the non-radiative relaxation of the excited state.[42,55–58] This agrees as well with the increase of the fluorescence quantum yield observed in alcohols on going from MeOH to PeOH, *i.e.* on decreasing the hydrogen-bond donating ability of the solvent.

Contrary to the absorption spectrum, the fluorescence band shape is independent of the chromophore concentration. Similarly, the fluorescence quantum yield measured at different HelR concentrations is essentially constant within the limit of error and is around 0.026, 0.019, and 0.016 for HelPr, HelMe and HelOH, respectively. It can thus be concluded that the fluorescence quantum yield of aggregated and non-aggregated HelR are very similar. This contrasts with many ionic dyes, such as those of the xanthene family, for which aggregation leads to a strong decrease of the fluorescence quantum yield.[59–61] As discussed later, this probably stems for the structure of the aggregates.

In contrast to the fluorescence quantum yield, the fluorescence dynamics in aqueous solution becomes longer with increasing concentration (Fig. 6). The time profiles measured at different HelR concentrations could be analyzed globally using the convolution of the IRF and a biexponential function with the time constants listed in Table 3. The biphasic nature of the decay indicates the presence of two emitting species. As the slow decay component increases with HelR concentration, its lifetime can be attributed to the aggregates, whereas the short lifetime can be ascribed to monomeric HelR dyes. The increase of the monomer lifetime on going from H_2O to D_2O confirms the role of hydrogen bonds in the non-radiative transition from the S_1
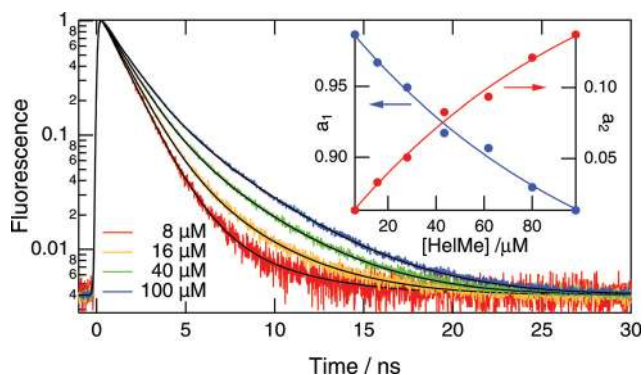
Fig. 6 Intensity-normalized fluorescence decays of (*rac*)-HelMe at different concentrations in PBS solution. Inset: concentration dependence of the amplitudes, a_i, obtained from biexponential analysis.

Fig. 7 (A) Excitation anisotropy and absorption spectra of (*rac*)-HelPr in a polymer film, and (B) time profiles of the fluorescence anisotropy at 650 nm measured with (rac)-HelMe in aqueous buffer solution and ethanol upon 400 nm excitation and best fits.

state. Most probably, the hydrogen-bonding interaction occurs at the methoxy-oxygen atoms. The coupling with the solvent should become stronger in the S_1 state because of the increase of the electron density at the oxygen atoms associated with the charge transfer character of the $S_1 \leftarrow S_0$ transition (Fig. 2). Such an increase of the hydrogen-bonding interaction upon excitation has been shown to strongly favour hydrogen bond assisted non-radiative deactivation.[42,55–58]

TA spectra of some of the HelR dyes in aqueous solutions have also been measured (Fig. 4B). At this concentration (<0.3 mM), the fraction of aggregates was higher than that of free dyes. No significant difference in the shape of the TA spectra compared with those measured in organic solvents could be observed, apart from a higher relative intensity of the positive TA bands. The TA spectra also exhibit some early dynamics that can be ascribed to vibrational relaxation and then decay on the nanosecond timescale in agreement with the fluorescence lifetime.

Further evidence of aggregation in aqueous solution can be obtained from the decay of the fluorescence anisotropy, $r(t)$, which, as it occurs *via* the reorientational motion of the emitter, depends on its size.[62] The anisotropy decays of (*rac*)-HelMe in PBS and EtOH, two media of similar viscosity, *i.e.* $\eta \sim 1$ cP at 20 °C, are depicted in Fig. 7B. The poor signal to noise (S/N) ratio of the data arises from the very small anisotropy of the fluorescence upon 400 nm excitation as illustrated by the fluorescence excitation anisotropy spectrum of (*rac*)-HelPr in a poly(methyl methacrylate-*co*-butyl methacrylate) film (Fig. 7A).

The small initial anisotropy in Fig. 7B arises from the angle between the $S_1 \rightarrow S_0$ transition dipole moment and that responsible for absorption at 400 nm. This value points to an angle of 50°, whereas TD-DFT calculations predict angles of 90° between the $S_1 \leftarrow S_0$ and $S_2 \leftarrow S_0$ dipoles and of 28° between the $S_1 \leftarrow S_0$ and $S_3 \leftarrow S_0$ dipoles. As vibronic coupling can lead to a considerable mixing of the S_2 and S_3 electronic states,[63,64] the small anisotropy upon 400 nm excitation is not surprising. On the other hand, Fig. 7A shows that the fluorescence anisotropy upon excitation in the $S_1 \leftarrow S_0$ band is close to the maximum of 0.4 for parallel transition dipoles. The dye concentration in these fluorescence up-conversion measurements was higher, ~0.2 mM, than for TCSPC and steady-state experiments, and therefore the aggregate form predominates in aqueous solution.
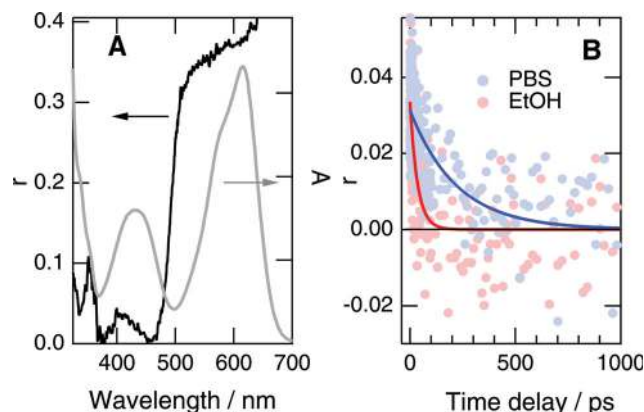
Despite the small S/N ratio, a slower decay of the anisotropy is evident in aqueous solution. Both anisotropy time profiles can be reproduced with an exponential function decaying to zero with time constants of 200 ± 50 ps and 50 ± 10 ps in PBS solution and EtOH, respectively. Measurements with other HelR dyes confirm the slower anisotropy in aqueous solution. The anisotropy decay time in EtOH can be ascribed to the diffusional reorientation of the monomeric dye, whereas the longer decay time in aqueous buffer to that of the aggregate. The size of this aggregate cannot be directly determined from this time constant as the latter not only depends on the volume but also on the shape of the rotator.[62]

The equilibrium between the monomeric, M, and aggregated, A, forms of an enantiopure HelR dye can be described as:

$$n\text{M} \rightleftharpoons \text{A} \quad \text{with } K_e = \frac{[\text{A}]}{[\text{M}]^n} \quad (1)$$
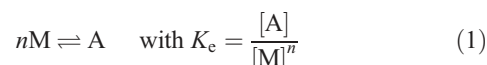
where n is the number of molecules in the aggregate and K_e is the equilibrium constant for the aggregation of enantiopure dyes.

As the total HelR concentration is [HelR] = [M] + n[A], the relationships between the concentration of each form and [HelR] are:

$$[\text{HelR}] = [\text{M}] + nK_e[\text{M}]^n \quad (2)$$

$$[\text{HelR}] = ([\text{A}]/K_e)^{1/n} + n[\text{A}] \quad (3)$$

Since the contributions of the short and long decay components of the fluorescence dynamics, *i.e.* the amplitude multiplied by the lifetime, are proportional to [M] and [A], respectively, their dependence on the total dye concentration can be analyzed with eqn (2) to extract K_e and n (Fig. 8, Table 4). An aggregation number of 2 has been found for all HelR dyes except for (*M*)- and (*P*)-HelPr. This indicates that, for all but these two, a simple dimerization is taking place. However, the fluorescence time profiles measured at different HelR concentrations cannot be perfectly reproduced using two global time constants. Indeed, the analysis of each individual profile results
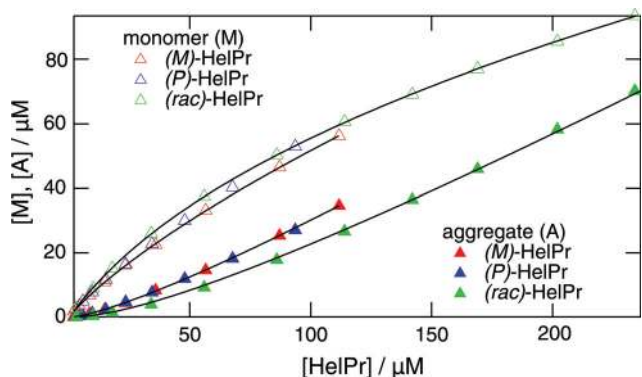
Fig. 8 Concentration of the aggregated, [A], and non-aggregated, [M], HelPr in aqueous buffer solution as a function of the total HelPr concentration and best fits of equations (2) and (5).

to somewhat different lifetimes. Therefore, the presence of larger aggregates cannot be excluded.

Heterochiral aggregates, A_{+-}, can additionally be formed in racemic mixtures:

$$p M_+ + m M_- \rightleftharpoons A_{+-} \quad \text{with } K_r = \frac{[A_{+-}]}{[M_+]^n [M_-]^n} \quad (4)$$
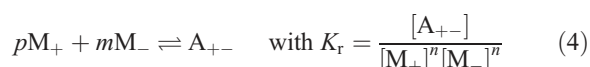
In this case, the total HelR concentration is:

$$[\text{HelR}] = [M_+] + [M_-] + n_+[A_+] + n_-[A_-] + (p+m)[A_{+-}] \quad (5)$$

This equation can be simplified since the homochiral aggregates, A_+ and A_-, have, as expected, the same aggregation constant, K_e, and number, n (Table 4). Moreover, if we assume that $p = m$, eqn (5) becomes:

$$[\text{HelR}] = 2[M] + 2nK_e[M]^n + 2mK_r[M]^{2m} \quad (6)$$

To determine K_r and m, the concentration dependence of the slow and fast contributions to the fluorescence decay measured with the racemic HelR dyes was analyzed using eqn (5) and the n and K_e values obtained with the enantiopure compounds (Table 4). This procedure worked well with HelMe and HelPr, but did not yield physically realistic values with HelOH. Most probably, the above model is too simplistic for this dye. For example, interactions between homochiral aggregates of opposite chirality, that have been neglected here, might be significant with HelOH. For the other two HelR dyes, Table 4 reveals that the heterochiral aggregates are dimers as well and that their aggregation constant K_r is substantially larger that for homochiral

Table 4 Aggregation equilibrium constant, K_e, and aggregation number, n and m for the HelR dyes in aqueous solution

Molecule		n	$2m$	K_e	K_r
HelMe	(M)-	2		5.7×10^3	
	(P)-	2		5.5×10^3	
	rac-		2		1×10^4
HelPr	(M)-	1.6		230	
	(P)-	1.5		260	
	rac-		2		3.1×10^4
HelOH	(M)-	2		4.3×10^3	
	(P)-	2		4.7×10^3	

dimers, K_e. This difference in the aggregation constant between enantiopure and racemic aggregates reveals that heterochiral complexes are more stable than homochiral ones. This is a common property of chiral systems and has been reported for other homochiral and heterochiral complexes.[65] Two dyes of opposite chirality can form a more compact dimer than two molecules of the same chirality, favouring stabilizing intermolecular interactions. The bulky propyl groups probably minimize these interactions between homochiral HelPr dyes. Because of this, dimers without a well-defined geometry might be formed, leading to an apparent n value of 1.5. With two HelPr of opposite chirality, this problem might be just smaller enough to enable the formation of a more stable dimer with a better-defined geometry.

The small changes in the absorption spectra observed with increasing HelR concentration originate from the slightly different absorption spectra of monomers and dimers. As the relative concentration of these two forms is known from the fluorescence decays, their respective absorption spectrum can be determined. Fig. 9 shows the calculated spectra of the monomeric and homo- and heterochiral dimeric forms of the HelR dyes. The validity of the results is comforted by the fact that the calculated spectra of the monomers are identical to those measured in organic solvents, where aggregation does not take place, and are the same for enantiopure and racemic HelR solutions. The absorption spectra of the dimers are characterized by a band around 600 nm with two maxima, and a substantial red shift of the second band compared to that of the monomers. The absorption spectra of the homo- and heterodimers of HelMe and HelOH are almost identical and the energy spacing between the two maxima of the 600 nm band is around 940 cm^{-1}. On the other hand, the absorption spectra of the homo- and heterodimers of HelPr differ
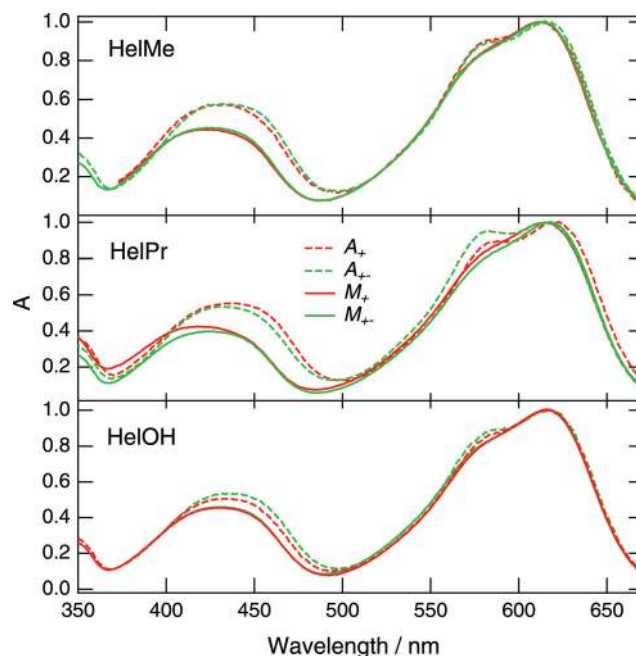
Fig. 9 Calculated absorption spectra of the aggregated, A, and non-aggregated, M, forms of (P)-HelR, +, and (rac)-HelR, +−, in aqueous buffer solution.

by the relative intensity and energy splitting of the two maxima of the 600 nm band. This difference agrees with the above hypothesis of the homodimeric HelPr with a loose structure.

According to Kasha exciton theory,[66] information on the relative orientation of the dyes in an aggregate can be deduced from the effect of aggregation on the absorption spectrum. For example, the formation of H-aggregates with face-to-face constituents leads to a blue shift of the absorption band, whereas that of J-aggregated with a parallel end-to-end arrangement results to a red shift. On the other hand, a skew conformation appears as a splitting of the band. The size of the band shift and splitting reflects the interaction between the transition dipole moments of the constituents and thus depends on their magnitude, distance and relative orientation. Information on the nature of the aggregate can also be obtained from the fluorescence. Indeed, H-aggregates are non-fluorescent because of a negligibly small radiative rate constant, k_r, whereas J-aggregates fluoresce and have a larger k_r than the constituents. Furthermore, their emission band is red shifted relative to that of the monomer. Finally, skew aggregates are fluorescent with a k_r that depends on the skew angle. In the present case, the lowest excited state of the dimer should be at approximately the same energy as that of the monomer, as suggested by the location of the low energy maximum of the 600 nm band that coincides well with the band maximum of the monomer and by the very similar fluorescence spectra of both monomer and dimer. However, the radiative rate constant of the dimer is substantially smaller than that of the monomer as reflected by the different fluorescence lifetimes (Table 3), as both forms have the same fluorescence quantum yield. The second absorption band around 425 nm is even more affected by aggregation, as this effect leads to a red shift and a higher intensity of the band. As mentioned above, this band arises from both $S_2 \leftarrow S_0$ and $S_3 \leftarrow S_0$ transitions with the dipole moments aligned along the x- and y-axis, respectively (Fig. 2). Dimerization should thus lead to different magnitude of the excitonic interaction between these transition dipoles. Clearly the dimers are neither H nor J dimers, but could rather have a skew conformation or a conformation between those of H and J dimers, where the constituents have a displaced face-to-face configuration. More insight into the structure of these dimers would need quantum chemical calculations that are beyond the scope of this investigation.

Conclusions

Here we have reported on the photophysical properties of new chiral cationic dyes that emits in the near infrared region. The results reveal that aggregation is an important feature of [4]helicene dyes in aqueous solution. Whereas aggregation substantially affects the fluorescence lifetimes and anisotropy decay, it has little or no effect on the electronic absorption and emission spectra and on the fluorescence quantum yield. Aggregation does not take place in organic solvents, as testified by a single exponential fluorescence decay.

Since their fluorescence quantum yield varies between 0.01 and 0.2, these compounds could be applicable as near infrared probe dyes. Apart from their aggregation in aqueous solution, the photophysical properties of these helicenes are relatively insensitive to the solvent properties, the exception being a

shortening of the fluorescence quantum yield and lifetime in with increasing hydrogen-bond donating properties of the solvent. This property, together with their chirality and relative hydrophobicity could make these dyes useful for probing biological molecules such as nucleic acids and proteins.

Notes and references

1 R. W. Sinkeldam, N. J. Greco and Y. Tor, Fluorescent analogs of biomolecular building blocks: design, properties, and applications, *Chem. Rev.*, 2010, **110**, 2579–2619.

2 C. L. Amiot, S. Xu, S. Liang, L. Pan and J. X. Zhao, Near-infrared fluorescent materials for sensing of biological targets, *Sensors*, 2008, **8**, 3082–3105.

3 J. V. Frangioni, *In vivo* near-infrared fluorescence imaging, *Curr. Opin. Chem. Biol.*, 2003, **7**, 626–634.

4 X. He, J. Gao, S. S. Gambhir and Z. Cheng, Near-infrared fluorescent nanoprobes for cancer molecular imaging: status and challenges, *Trends Mol. Med.*, 2010, **16**, 574–583.

5 R. Weissleder, C.-H. Tung, U. Mahmood and A. Bogdanov, Jr., *In vivo* imaging of tumors with protease-activated near-infrared fluorescent probes, *Nat. Biotechnol.*, 1999, **17**, 375–378.

6 S. A. Soper, Q. L. Mattingly and P. Vegunta, Photon burst detection of single near-infrared fluorescent molecules, *Anal. Chem.*, 1993, **65**, 740–747.

7 B. W. Laursen and F. C. Krebs, Synthesis of a triazatriangulenium salt, *Angew. Chem., Int. Ed.*, 2000, **39**, 3432–3434.

8 B. W. Laursen and F. C. Krebs, Synthesis, structure, and properties of azatriangulenium salts, *Chem.–Eur. J.*, 2001, **7**, 1773–1783.

9 C. Herse, D. Bas, F. C. Krebs, T. Bürgi, J. Weber, T. Wesolowski, B. W. Laursen and J. Lacour, A highly configurationally stable (4)heterohelicenium cation, *Angew. Chem., Int. Ed.*, 2003, **42**, 3162.

10 B. Laleu, P. Mobian, C. Herse, B. W. Laursen, G. Hopfgartner, G. Bernardinelli and J. Lacour, Resolution of [4]heterohelicenium dyes with unprecedented Pummerer-like chemistry, *Angew. Chem., Int. Ed.*, 2005, **44**, 1879–1883.

11 P. Mobian, N. Banerji, G. Bernardinelli and J. Lacour, Towards the stereoselective synthesis of inherently chiral pseudorotaxanes, *Org. Biomol. Chem.*, 2006, **4**, 224–231.

12 C. Villani, B. Laleu, P. Mobian and J. Lacour, Effective HPLC resolution of [4]heterohelicenium dyes on chiral stationary phases using reversed phase eluents, *Chirality*, 2007, **19**, 601–606.

13 D. Conreaux, N. Mehanna, C. Herse and J. Lacour, From cationic to anionic helicenes: new reactivity through umpolung, *J. Org. Chem.*, 2011, **76**, 2716–2722.

14 N. Mehanna, S. Grass and J. Lacour, On the surprising loss of chromatographic separation on silica gel of [4]helicene sulfoxide diastereoisomers upon increasing compound polarity, *Chirality*, 2011 submitted.

15 T. J. Wigglesworth, D. Sud, T. B. Norsten, V. S. Lekhi and N. R. Branda, Chiral discrimination in photochromic helicenes, *J. Am. Chem. Soc.*, 2005, **127**, 7272–7273.

16 T. Okuyama, Y. Tani, K. Miyake and Y. Yokoyama, Chiral helicenoid diarylethene with large change in specific optical rotation by photochromism, *J. Org. Chem.*, 2007, **72**, 1634–1638.

17 B. Busson and A. Tadjeddine, Chiral specificity of doubly resonant sum-frequency generation in an anisotropic thin film, *J. Phys. Chem. C*, 2008, **112**, 11813–11821.

18 F. Furche, R. Ahlrichs, C. Wachsmann, E. Weber, A. Sobanski, F. Voegtle and S. Grimme, Circular dichroism of helicenes investigated by time-dependent density functional theory, *J. Am. Chem. Soc.*, 2000, **122**, 1717–1724.

19 J. Autschbach, T. Ziegler, S. J. A. van Gisbergen and E. J. Baerends, Chiroptical properties from time-dependent density functional theory. I. Circular dichroism spectra of organic molecules, *J. Chem. Phys.*, 2002, **116**, 6930–6940.

20 E. Botek, J.-M. Andre, B. Champagne, T. Verbiest and A. Persoons, Mixed electric–magnetic second-order nonlinear optical response of helicenes, *J. Chem. Phys.*, 2005, **122**, 234713–234716.

21 J. Guin, C. Besnard and J. Lacour, Synthesis, resolution, and stabilities of a cationic chromenoxanthene [4]helicene, *Org. Lett.*, 2010, **12**, 1748–1751.

22 Y. Xu, Y. X. Zhang, H. Sugiyama, T. Umano, H. Osuga and K. Tanaka, (P)-Helicene displays chiral selection in binding to Z-DNA, *J. Am. Chem. Soc.*, 2004, **126**, 6566–6567.

23 S. Honzawa, H. Okubo, S. Anzai, M. Yamaguchi, K. Tsumoto and I. Kumagai, Chiral recognition in the binding of helicenediamine to double strand DNA: interactions between low molecular weight helical compounds and a helical polymer, *Bioorg. Med. Chem.*, 2002, **10**, 3213–3218.

24 R. Passeri, A. G. Gaetano, F. Elisei, L. Latterini, T. Caronna, F. Fontana and S. I. Natali, Photophysical properties of N-alkylated azahelicene derivatives as DNA intercalators: counterion effects, *Photochem. Photobiol. Sci.*, 2009, **8**, 1574–1582.

25 V. A. Bloomfield, D. M. Crothers and I. Tinoco, Jr., *Nucleic Acids: Structures, Properties and Functions*, University Science Books, 2000.

26 M. A. Shcherbina, X.-b. Zeng, T. Tadjiev, G. Ungar, S. H. Eichhorn, K. E. S. Phillips and T. J. Katz, Hollow six-stranded helical columns of a helicene, *Angew. Chem., Int. Ed.*, 2009, **48**, 7837–7840.

27 K. E. S. Phillips, T. J. Katz, S. Jockusch, A. J. Lovinger and N. J. Turro, Synthesis and properties of an aggregating heterocyclic helicene, *J. Am. Chem. Soc.*, 2001, **123**, 11899–11907.

28 R. E. Franklin and R. G. Gosling, Molecular configuration in sodium thymonucleate, *Nature*, 1953, **171**, 740–741.

29 S. Machida, K. Sano, K. Sunohara, Y. Kawata and Y. Mori, The novel texture of a liquid crystal induced by poly-benzyl-L-glutamate chemical reaction alignment (CRA) film, *J. Chem. Soc., Chem. Commun.*, 1992, 1628–1629.

30 J. R. C. van der Maarel, D. E. Woessner and M. E. Merritt, Extremely slow counterion dynamics in xanthan liquid crystal through ^{23}Na and ^{14}N NMR, *J. Phys. Chem. B*, 2002, **106**, 3864–3871.

31 Z. An, Y. Yasui, T. Togashi, T. Adschiri, S. Hitosugi, H. Isobe, T. Higuchi, M. Shimomura and M. Yamaguchi, Reversible aggregation and deaggregation of helicene-grafted chiral silica nanoparticles induced by aromatic solvents, *Chem. Lett.*, 2010, **39**, 1004–1005.

32 K. Nakamura, H. Okubo and M. Yamaguchi, Synthesis and self-aggregation of cyclic alkynes containing helicene, *Org. Lett.*, 2001, **3**, 1097–1099.

33 N. Fukawa, T. Osaka, K. Noguchi and K. Tanaka, Asymmetric synthesis and photophysical properties of benzopyrano- or naphthopyrano-fused helical phosphafluorenes, *Org. Lett.*, 2010, **12**, 1324–1327.

34 S. Abbate, T. Caronna, A. Longo, A. Ruggirello and L. V. Turco, Study of confined 5-aza[5]helicene in ytterbium(III) bis(2-ethylhexyl) sulfosuccinate reversed micelles, *J. Phys. Chem. B*, 2007, **111**, 4089–4097.

35 H. Görner, C. Stammel and J. Mattay, Excited state behavior of pentahelicene dinitriles, *J. Photochem. Photobiol., A*, 1999, **120**, 171–179.

36 M. Sapir and D. E. Vander, Intersystem crossing in the helicenes, *Chem. Phys. Lett.*, 1975, **36**, 108–110.

37 K. Schmidt, S. Brovelli, V. Coropceanu, D. Beljonne, J. Cornil, C. Bazzini, T. Caronna, R. Tubino, F. Meinardi, Z. Shuai and J.-L. Bredas, Intersystem crossing processes in nonplanar aromatic heterocyclic molecules, *J. Phys. Chem. A*, 2007, **111**, 10490–10499.

38 B. W. Laursen, PhD thesis, 2001, Risø National Laboratory and University of Copenhagen.

39 G. Solladie, J. Hutt and A. Girardin, Improved preparation of optically active methyl p-tolyl sulfoxide, *Synthesis*, 1987, 173.

40 M. C. Carreño, Applications of sulfoxides to asymmetric synthesis of biologically active compounds, *Chem. Rev.*, 1995, **95**, 1717–1760.

41 R. Sens and K. H. Drexhage, Fluorescence quantum yield of oxazine and carbazine laser dyes, *J. Lumin.*, 1981, **24–25**, 709–712.

42 A. Fürstenberg and E. Vauthey, Excited state dynamics of the fluorescent probe Lucifer Yellow in liquid solutions in heterogeneous media, *Photochem. Photobiol. Sci.*, 2005, **4**, 260–267.

43 A. Morandeira, L. Engeli and E. Vauthey, Ultrafast charge recombination of photogenerated ion pairs to an electronic excited state, *J. Phys. Chem. A*, 2002, **106**, 4833–4837.

44 G. Duvanel, J. Grilj, H. Chaumeil, P. Jacques and E. Vauthey, Ultrafast excited-state dynamics of a series of zwitterionic pyridinium phenoxides with increasing sterical hindering, *Photochem. Photobiol. Sci.*, 2010, **9**, 908–915.

45 G. Duvanel, N. Banerji and E. Vauthey, Excited-state dynamics of donor–acceptor bridged systems containing a boron-dipyrromethene chromophore: interplay between charge separation and reorientational motion, *J. Phys. Chem. A*, 2007, **111**, 5361–5369.

46 N. Banerji, G. Duvanel, A. Perez-Velasco, S. Maity, N. Sakai, S. Matile and E. Vauthey, Excited-state dynamics of hybrid multichromophoric systems: toward an excitation wavelength control of the charge separation pathways, *J. Phys. Chem. A*, 2009, **113**, 8202–8212.

47 J. P. Perdew, Density-functional approximation for the correlation energy of the inhomogeneous electron gas, *Phys. Rev. B*, 1986, **33**, 8822–8824.

48 A. Schäfer, H. Horn and R. Ahlrichs, Fully optimized contracted Gaussian basis sets for atoms Li to K, *J. Chem. Phys.*, 1992, **97**, 2571–2577.

49 R. Bauernschmitt and R. Ahlrichs, Treatment of electronic excitations within the adiabatic approximation of time dependent density functional theory, *Chem. Phys. Lett.*, 1996, **256**, 454–464.

50 R. Ahlrichs, M. Bär and M. Häser, Electronic structure calculations on workstation computers: the program system turbomole, *Chem. Phys. Lett.*, 1989, **162**, 165–169.

51 N. Mehanna, PhD thesis, 2010, University of Geneva.

52 T. Förster, Electron spectra of coupled molecules, *Pure Appl. Chem.*, 1962, **4**, 121–134.

53 J. B. Birks, Excimers, *Rep. Prog. Phys.*, 1975, **38**, 903–974.

54 P. Suppan and N. Ghoneim, *Solvatochromism*, The Royal Society of Chemistry, Cambridge, 1997.

55 S. R. Flom and P. F. Barbara, Proton transfer and hydrogen bonding in the internal conversion of S1 anthraquinones, *J. Phys. Chem.*, 1985, **89**, 4489–4494.

56 H. Inoue, M. Hida, N. Nakashima and K. Yoshihara, Picosecond fluorescence lifetimes of anthraquinone derivatives. Radiationless deactivation *via* intra- and intermolecular hydrogen bonds, *J. Phys. Chem.*, 1982, **86**, 3184–3188.

57 P. S. Sherin, J. Grilj, Y. P. Tsentalovitch and E. Vauthey, Ultrafast excited-state dynamics of kynurenine, a UV filter of the human eye, *J. Phys. Chem. B*, 2009, **113**, 4953–4962.

58 P. Fita, M. Fedoseeva and E. Vauthey, Ultrafast excited-state dynamics of eosin B: a potential probe of the hydrogen-bonding properties of the environment, *J. Phys. Chem. A*, 2011, **115**, 2465–2470.

59 A. Penzkofer and Y. Lu, Fluorescence quenching of rhodamine 6G in methanol at high concentration, *Chem. Phys.*, 1986, **103**, 399–405.

60 O. Valdes-Aguilera and D. C. Neckers, Aggregation phenomena in xanthene dyes, *Acc. Chem. Res.*, 1989, **22**, 171–177.

61 P. Fita, M. Fedoseeva and E. Vauthey, Hydrogen-bond-assisted excited-state deactivation at liquid/water interfaces, *Langmuir*, 2011, **27**, 4645–4652.

62 G. R. Fleming, *Chemical Applications of Ultrafast Spectroscopy*, Oxford University Press, New York, 1986.

63 N. Sarkar, S. Takeuchi and T. Tahara, Vibronic relaxation of polyatomic molecule in nonpolar solvent: femtosecond anisotropy/intensity measurements of the S_n and S_1 fluorescence of tetracene, *J. Phys. Chem. A*, 1999, **103**, 4808–4814.

64 A. Pigliucci, G. Duvanel, M. L. Lawson Daku and E. Vauthey, Investigation of the influence of solute–solvent interactions on the vibrational energy relaxation dynamics of large molecules in liquids, *J. Phys. Chem. A*, 2007, **111**, 6135–6145.

65 E. L. Eliel, S. H. Wilen and L. N. Mander, *Stereochemistry of Organic Compounds*, Wiley, 1994.

66 M. Kasha, H. R. Rawls and M. A. El-Bayoumi, The exciton model in molecular spectroscopy, *Pure Appl. Chem.*, 1965, **11**, 371–392.